

RECURRENT DISTANCE-ENCODING NEURAL NETWORKS FOR GRAPH REPRESENTATION LEARNING

Yuhui Ding^{1,*} Antonio Orvieto² Bobby He¹ Thomas Hofmann¹

¹ETHZ, Zürich, Switzerland ²ELLIS Institute Tübingen, MPI-IS, Tübingen AI Center, Tübingen, Germany

*yuhui.ding@inf.ethz.ch

ABSTRACT

Graph neural networks based on iterative one-hop message passing have been shown to struggle in harnessing information from distant nodes effectively. Conversely, graph transformers allow each node to attend to all other nodes directly, but suffer from high computational complexity and have to rely on ad-hoc positional encoding to bake in the graph inductive bias. In this paper, we propose a new architecture to reconcile these challenges. Our approach stems from the recent breakthroughs in long-range modeling provided by deep state-space models on sequential data: for a given target node, our model aggregates other nodes by their shortest distances to the target and uses a parallelizable linear recurrent network over the chain of distances to provide a natural encoding of its neighborhood structure. With no need for positional encoding, we empirically show that the performance of our model is highly competitive compared with that of state-of-the-art graph transformers on various benchmarks, at a drastically reduced computational complexity. In addition, we show that our model is theoretically more expressive than one-hop message passing neural networks¹.

1 INTRODUCTION

Graphs are ubiquitous for representing complex interactions between individual entities, such as in social networks (Tang et al., 2009), recommender systems (Ying et al., 2018) and molecules (Gilmer et al., 2017), and have thus attracted a lot of interest from researchers seeking to apply deep learning to graph data. Message passing neural networks (MPNNs) (Gilmer et al., 2017) have been the dominant approach in this field. These models iteratively update the representation of a target node by aggregating the representations of its neighbors. Despite progress on semi-supervised node classification tasks (Kipf & Welling, 2017; Veličković et al., 2018), MPNNs have been shown to have intrinsic limitations. Firstly, the expressive power of any MPNN is upper bounded by the Weisfeiler-Lehman graph isomorphism test (1-WL) (Xu et al., 2019). Moreover, to utilize the information from a node that is k hops away from the target node, an MPNN needs to perform k rounds of message passing. As a result, the receptive field for the target node grows exponentially with k , including many duplicates of nodes that are close to the target node. The information from an exponentially growing receptive field is compressed into a fixed-size representation, making it difficult to effectively harness the information of the distant nodes (a.k.a. over-squashing (Alon & Yahav, 2021; Topping et al., 2022)). These limitations may hinder the application of MPNNs to tasks that require reasoning between distant nodes.

Recently, inspired by the success of attention-based transformer architectures in modeling natural languages (Vaswani et al., 2017; Devlin et al., 2019) and images (Dosovitskiy et al., 2021), several works have adapted transformers for graph representation learning (Ying et al., 2021; Kim et al., 2022; Chen et al., 2022; Zhang et al., 2023). Graph transformers allow each node to attend to all other nodes directly through a global attention mechanism, and therefore make information flow between distant nodes easier. However, a naive implementation of a global attention mechanism alone doesn't encode any structural information about the underlying graph. As a result, state-of-the-art graph transformers rely on ad hoc positional encoding (e.g., eigenvectors of the graph Laplacian) as extra features to incorporate the graph inductive bias. There is no consensus yet on the

¹Code will be available at <https://github.com/skeletondyh/GRED>

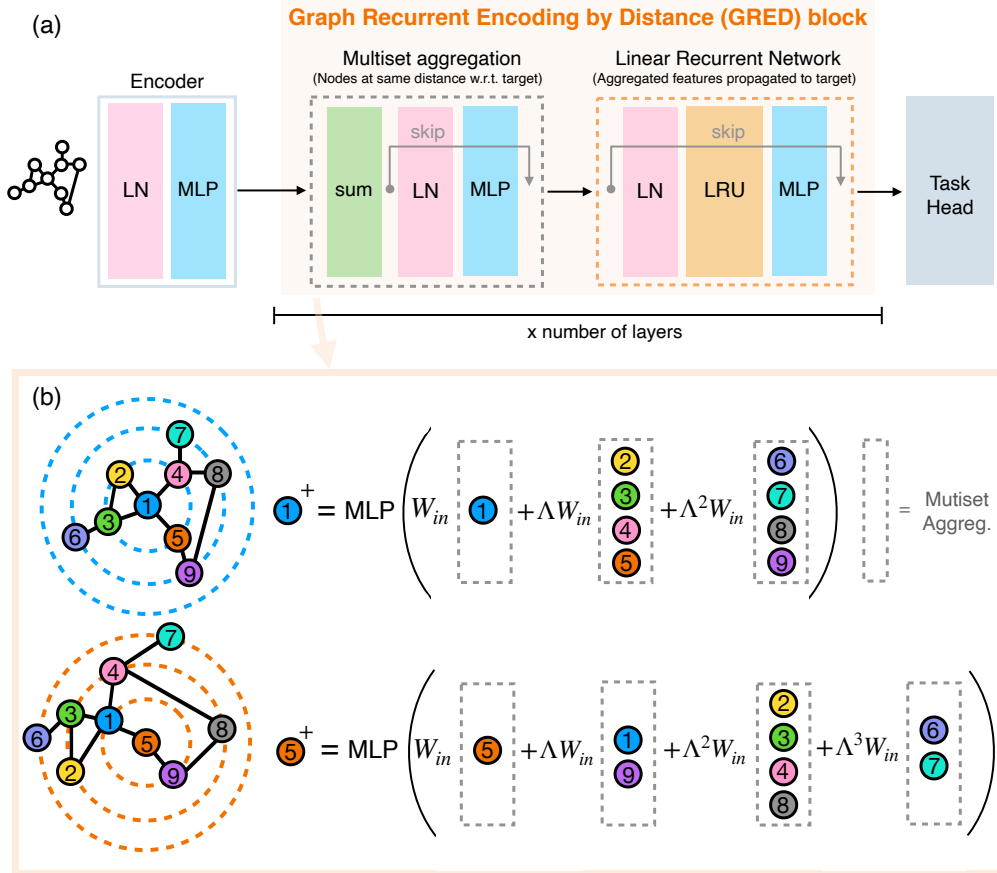


Figure 1: (a) Sketch of the architecture. MLPs and Layer Normalization operate independently at each node or node multiset. Information is propagated along edges through a linear RNN – specifically an LRU (Orvieto et al., 2023b). (b) Depiction of the GRED layer operation for two target nodes. The gray rectangular boxes indicate the application of multiset aggregation. Finally, the new representation for the target node is computed from the RNN output through an MLP.

optimal type of positional encoding, and what positional encoding to use is often a hyper-parameter that needs to be carefully tuned (Rampásek et al., 2022). Besides, while graph transformers have empirically shown improvement on some graph benchmarks compared with classical MPNNs, the former has a much higher computational complexity (Ying et al., 2021).

Captivated by the above challenges and the need for powerful, theoretically sound and computationally efficient approaches to graph representation learning, we propose a new model, Graph Recurrent Encoding by Distance (GRED). To learn the representation for a target node, our model categorizes all other nodes into multiple sets according to their shortest distances to the target node. The first component of a GRED layer is a permutation-invariant neural network (Zaheer et al., 2017) which generates a representation for each set of nodes that share the same shortest distance to the target node. The second component of a GRED layer is a linear recurrent neural network (Orvieto et al., 2023b) to encode the sequence of the set representations, starting from the set with the maximum shortest distance towards the target node. Since the order of the sequence is naturally encoded by the recurrent neural network, our model can encode the shortest distance of each set and thus the neighborhood structure of the target node. The architecture of GRED is illustrated in Figure 1.

The combination of a permutation-invariant neural network and a linear recurrent neural network brings several advantages to our model compared to existing approaches. First, the recurrent neural network allows the target node to effectively harness the information from distant nodes, and at the same time encodes the hierarchical structure of its neighborhood. As a result, our model doesn't require any positional encoding, unlike graph transformers. Second, the expressive power of the linear recurrent neural network strengthens that of the permutation-invariant neural network, making our model strictly more expressive than any one-hop MPNN (see Section 4 for detailed analysis). Third, both the linear recurrent neural network and the permutation-invariant neural network enable fast

parallelizable computation, making our model significantly more efficient than graph transformers. We evaluate our model on a series of graph benchmarks to support its efficacy. The performance of our model is consistently better than that of existing MPNNs and is also competitive compared with that of the state-of-the-art graph transformers, with drastically reduced computation time.

To summarize, the main contributions of our paper are as follows:

1. We propose a principled new architecture for graph representation learning to more effectively and efficiently utilize the information of large neighborhoods. The proposed architecture consists of linear recurrent neural networks interleaved with permutation-invariant neural networks.
2. Based on the injectivity of linear recurrent neural networks, we theoretically prove that the expressiveness of our proposed architecture is strictly greater than that of one-hop MPNNs.
3. We empirically show that the performance of our model is significantly better than that of MPNNs and comparable to that of state-of-the-art graph transformers, with no need for positional encoding. We also show that our model takes significantly less training time than graph transformers.

2 RELATED WORK

We review below recent literature on increasing MPNN’s receptive field as well as current trends in recurrent models for long-range reasoning on sequential data.

Increasing the receptive field of MPNNs. There is a rich literature on using higher hop information for MPNNs. Among them, MixHop (Abu-El-Haija et al., 2019) uses powers of the normalized adjacency matrix to access k -hop nodes. k -hop GNN (Nikolentzos et al., 2020) iteratively applies MLPs to combine two consecutive hops and propagates information towards the target node. While they have shown higher hop information can improve the expressiveness of MPNNs, they have the over-squashing problem (Topping et al., 2022) due to neighborhood mixing. SPN (Abboud et al., 2022) first aggregates nodes of the same hop and then combines hop representations using weighted summation. Although SPN alleviates over-squashing empirically, weighted summation of hops cannot guarantee the expressiveness of the model. Recently, Graph transformers (Ying et al., 2021; Chen et al., 2022; Rampásek et al., 2022; Zhang et al., 2023; Wu et al., 2021) have attracted a lot of attention because the global attention mechanism allows each node to directly attend to all other nodes. To bake in the graph structural information, graph transformers typically use positional encoding (Li et al., 2020; Dwivedi et al., 2022b) as extra node features. Specifically, Graphormer (Ying et al., 2021) adds learnable bias to the attention matrix to make the model aware of nodes with different shortest distances. However, the sequential order of the distances is not encoded into the model and Graphormer still needs local node degrees as extra input node features. SAT (Chen et al., 2022) and GraphTrans (Wu et al., 2021) stack message passing layers and self-attention layers together to obtain local information before the global attention. GPS (Rampásek et al., 2022) applies the linear attention (Choromanski et al., 2021) to graph transformers and empirically investigates different configurations of positional encoding. Zhang et al. (2023) theoretically proves the expressive power of different types of distance encoding regarding biconnectivity and proposes the use of resistance distance as relative positional encoding. GRIT (Ma et al., 2023a) utilizes learnable positional encoding initialized with random walk probabilities.

Issues with attention for long-range reasoning in sequential data. Efficient processing of long sequences is one of the paramount challenges in contemporary deep learning. Attention-based transformers (Vaswani et al., 2017) provide a scalable approach to sequential modeling but suffer from *quadratically increasing inference/memory complexity* as the sequence length grows. While many approaches exist to alleviate this issue, like efficient memory management (Dao et al., 2022; Dao, 2023) and architectural modifications (Wang et al., 2020; Kitaev et al., 2020; Child et al., 2019; Beltagy et al., 2020; Wu et al., 2020), the sequence length in modern large language models is usually kept to $2k/4k$ tokens for this reason (e.g. Llama2 (Touvron et al., 2023)). On top of high inference and memory cost, the attention mechanism often does not provide the correct *inductive bias* for long-range reasoning beyond text. Indeed, most transformers (including long-range/sparse variants, reduced complexity variants, or variants with other tricks) are often found to perform poorly in discovering long-range dependencies in data (Tay et al., 2021). Due to the issues outlined above, the community has witnessed in the last year the rise of new, drastically innovative, *recurrent* alternatives to the attention mechanism, named state-space models (SSMs). The first SSM, S4, was

introduced by Gu et al. (2022a) based on the theory of polynomial signal approximations (Gu et al., 2020; 2023), and since then, a plethora of variants have been proposed (Hasani et al., 2023; Gupta et al., 2022; Gu et al., 2022b; Smith et al., 2023; Peng et al., 2023). These models achieve remarkable performance, surpassing all modern attention-based transformer variants by an average 20% accuracy on challenging sequence classification tasks (Tay et al., 2021). Deep state-space models have reached outstanding results in various domains, including vision (Nguyen et al., 2022), audio (Goel et al., 2022), biological signals (Gu et al., 2022a), reinforcement learning (Lu et al., 2023) and online learning (Zucchet et al., 2023b). SSMs also were successfully applied to language modeling and are sometimes used in combination with attention (Fu et al., 2023; Wang et al., 2022; Ma et al., 2023b). At inference time, all SSMs coincide with a stack of linear Recurrent Neural Networks (RNNs), interleaved with position-wise MLPs and normalization layers. Such combination was recently shown to have fully expressiveness in modeling nonlinear dynamical systems (Orvieto et al., 2023a) – no recurrent nonlinearities are needed, since an MLP is placed at the output (cf. LSTMs (Hochreiter & Schmidhuber, 1997), GRUs (Chung et al., 2014)). Most importantly, the linearity of the RNNs allows for fast parallel processing using FFTs (Gu et al., 2022b) or parallel scans (Smith et al., 2023).

Linear recurrent unit. Among modern architectures for long-range reasoning based on recurrent modules, the simplest is perhaps Linear Recurrent Unit (LRU) (Orvieto et al., 2023b): while SSMs rely on the discretization of a structured continuous-time latent dynamical system, the LRU is directly designed for discrete-time systems (token sequences), and combines easy hyperparameter tuning with solid performance and scalability. The only difference between the LRU and the linearized standard RNN update $\mathbf{s}_k = \mathbf{A}\mathbf{s}_{k-1} + \mathbf{B}\mathbf{x}_k$ (\mathbf{x} is the input at a specific layer and \mathbf{s} is the hidden-state, then fed into a position-wise MLP) is (1) the system operates in the complex domain (required for expressivity, see discussion in Orvieto et al. (2023b)) (2) to enhance stability and prevent vanishing gradients, \mathbf{A} (diagonal) is learned using polar parametrization and log-transformed magnitude and phase (3) the recurrence is normalized through an extra optimizable parameter that scales the input to stabilize signal propagation. The parametrization of linear RNNs of (Orvieto et al., 2023b) was found to be effective also in surpassing deep LSTMs and GRUs (Zucchet et al., 2023a).

3 ARCHITECTURE

In this section, we present the GRED layer, which is the building unit of our architecture. We start with some preliminary notations and then describe how our layer computes node representations. Finally, we analyze its computational complexity. We defer the discussion on expressive power of our module to Section 4.

Preliminaries. Let $G = (V, E)$ denote an undirected and unweighted graph, where V denotes the set of nodes and E denotes the set of edges. For any two nodes $v, u \in V$, we use $d(v, u)$ to represent the shortest distance between v and u , and we let $d(v, v) = 0$. For each target node v , we categorize all other nodes into different hops according to their shortest distances to v :

$$\mathcal{N}_k(v) = \{u \mid d(v, u) = k\} \quad \text{for } k = 0, 1, \dots, K \quad (1)$$

where K can be the diameter of G or a hyper-parameter specified for the task in hand. $\{\mathcal{N}_k(v)\}_{k=1}^K$ can be obtained for each node $v \in V$ by running the Floyd–Warshall algorithm (Floyd, 1962; Warshall, 1962) in parallel once during data pre-processing.

Graph Recurrent Encoding by Distance (GRED). The input to the ℓ -th layer is the set of node representations $\{\mathbf{h}_v^{(\ell-1)} \in \mathbb{R}^d \mid v \in V\}$. To compute the output representation $\mathbf{h}_v^{(\ell)}$ for a generic target node v , the layer first generates a representation for each set of nodes that share the same shortest distance to v (grey dashed box in Figure 1):

$$\mathbf{x}_{v,k}^{(\ell)} = \text{AGG} \left(\{ \{ \mathbf{h}_u^{(\ell-1)} \mid u \in \mathcal{N}_k(v) \} \} \right) \quad \text{for } k = 0, 1, \dots, K \quad (2)$$

where AGG is an *injective* multiset function (Zaheer et al., 2017; Xu et al., 2019), which we parametrize, as usual in the literature (Zaheer et al., 2017; Xu et al., 2019; Feng et al., 2022), by two wide multi-layer perceptrons (MLPs)²:

$$\mathbf{x}_{v,k}^{(\ell)} = \text{MLP}_2 \left(\sum_{u \in \mathcal{N}_k(v)} \text{MLP}_1 \left(\mathbf{h}_u^{(\ell-1)} \right) \right). \quad (3)$$

²In practice, with just one hidden layer.

The sequence of the set representations $(\mathbf{x}_{v,0}^{(\ell)}, \mathbf{x}_{v,1}^{(\ell)}, \dots, \mathbf{x}_{v,K}^{(\ell)})$ is then encoded by a linear recurrent neural network (RNN), starting from $\mathbf{x}_{v,K}^{(\ell)}$ which is the farthest away from the target node to the target node itself, which gives:

$$\mathbf{s}_{v,k}^{(\ell)} = \mathbf{A}\mathbf{s}_{v,k-1}^{(\ell)} + \mathbf{B}\mathbf{x}_{v,K-k}^{(\ell)} \quad \text{for } k = 0, 1, \dots, K \quad (4)$$

where $\mathbf{s}_{v,k}^{(\ell)} \in \mathbb{R}^{d_s}$ represents the hidden state of the RNN and $\mathbf{s}_{v,-1}^{(\ell)} = \mathbf{0}$. $\mathbf{A} \in \mathbb{R}^{d_s \times d_s}$ denotes the state transition matrix and $\mathbf{B} \in \mathbb{R}^{d_s \times d}$ is a matrix to transform the input of the RNN³. It is well-known that wide enough linear RNNs can parameterize any convolutional filter over arbitrarily long input sequences (Li et al., 2022). Moreover, it was recently shown that, when interleaved with MLPs (placed at the recurrence output), a stack of linear RNNs can actually model any non-linear dynamical system (Orvieto et al., 2023a).

An important advantage of the linear recurrence, crucial for computational speed-up over sequential processing, is that it can be represented without loss of generality in a diagonal complex form (see discussion in Smith et al. (2023); Orvieto et al. (2023b)). Recall that, over the space of $d_s \times d_s$ non-diagonal real matrices, the set of non-diagonalizable (in the complex domain) matrices has measure zero (Bhatia, 2013). Hence, with probability one over random initializations, \mathbf{A} is diagonalizable, i.e. $\mathbf{A} = \mathbf{V}\mathbf{\Lambda}\mathbf{V}^{-1}$, where $\mathbf{\Lambda} = \text{diag}(\lambda_1, \dots, \lambda_{d_s}) \in \mathbb{C}^{d_s \times d_s}$ gathers the eigenvalues of \mathbf{A} , and columns of \mathbf{V} are the corresponding eigenvectors. Eq. (4) is equivalent to the following diagonal complex recurrence, up to a linear transformation of the hidden state \mathbf{s} which can be merged with the output projection \mathbf{W}_{out} (Eq. (6)):

$$\mathbf{s}_{v,k}^{(\ell)} = \mathbf{\Lambda}\mathbf{s}_{v,k-1}^{(\ell)} + \mathbf{W}_{\text{in}}\mathbf{x}_{v,K-k}^{(\ell)} \quad (5)$$

where $\mathbf{W}_{\text{in}} = \mathbf{V}^{-1}\mathbf{B} \in \mathbb{C}^{d_s \times d}$. Eq. (5) can be thought of as a *filter over the hops from the target node*, and the magnitudes of the eigenvalues $\mathbf{\Lambda}$ control how fast the filter decays as the shortest distance from the target node increases. Following the modern literature on long-range reasoning, we directly initialize (without loss in generality) the system in diagonal form (Gupta et al., 2022; Gu et al., 2022b), and train⁴ $\mathbf{\Lambda}$ and \mathbf{W}_{in} . To guarantee stability (eigenvalues in the unit disk), increased resolution at $|\lambda| \approx 1$ and strong signal propagation from distant nodes, we adopt the recently introduced LRU initialization and parametrization (Orvieto et al., 2023b), which also leverages parallel scans (Blelloch, 1990; Smith et al., 2023) to avoid computing \mathbf{s} sequentially on modern hardware.

The output representation $\mathbf{h}_v^{(\ell)}$ is generated by a non-linear transformation of the hidden state $\mathbf{s}_{v,K}^{(\ell)}$:

$$\mathbf{h}_v^{(\ell)} = \text{MLP} \left(\Re \left[\mathbf{W}_{\text{out}}\mathbf{s}_{v,K}^{(\ell)} \right] \right) \quad (6)$$

where $\mathbf{W}_{\text{out}} \in \mathbb{C}^{d \times d_s}$ is a trainable weight matrix and $\Re[\cdot]$ denotes the real part of a complex-valued vector. While sufficiently wide MLPs with one hidden layer can parametrize any non-linear map, following again the literature on state-space models we choose to place here a gated linear unit (GLU) (Dauphin et al., 2017): $\text{GLU}(\mathbf{x}) = (\mathbf{W}_1\mathbf{x}) \odot \sigma(\mathbf{W}_2\mathbf{x})$, with σ the sigmoid function.

The final architecture is composed of stacking several of such layers described above. In practice, we merge MLP_1 in Eq. (3) with the non-linear transformation in Eq. (6) at the previous layer (or at the encoding layer) to make the entire architecture more compact. We apply layer normalization to the input of both the MLP and the LRU, and also add skip connections. We provide a simplified implementation of a GRED layer in Appendix B

Computational complexity. For each shortest distance k , the complexity of aggregating representations of nodes from $\mathcal{N}_k(v)$ for every $v \in V$ is at most that of one round of message passing, which is $O(|E|)$. So the complexity of the first part of the computation of our layer (Eq. (3)) is less than $O(K|E|)$. In practice, since $\{\mathcal{N}_k(v)\}_{k=1}^K$ are pre-computed, computing Eq. (3) for every k can be parallelized. The sequential encoding of Eq. (5) has total complexity $O(K|V|)$. However, the linearity of the recurrence and the diagonal state transition matrix enable a parallel scan over the sequences, which further speeds up the computation. As a result, our model is highly efficient during training, as evidenced by our experimental results.

³Standard RNNs on sequences would have input \mathbf{x}_k and not \mathbf{x}_{K-k} . Here propagation starts from the farthest away nodes, and proceeds right-to-left as opposed to left-to-right, ending at the target node.

⁴As done in all state-space models Gu et al. (2022a); Smith et al. (2023), we do not optimize over the complex numbers but instead parameterize, for instance, real and imaginary components of \mathbf{W}_{in} as real parameters. The imaginary unit i is then used to aggregate the two components in the forward pass.

4 EXPRESSIVENESS ANALYSIS

We briefly recap the computation performed by a single GRED layer to update node representations $\{\mathbf{h}_u\}_{u \in V}$ (obtained via a previous layer or encoder) in some graph V . For each node $v \in V$ and distance k , we compute the k -hop neighbors $\mathcal{N}_k(v)$, and aggregate their representations using an injective multiset function AGG. The result is a sequence $(\mathbf{x}_{v,k})_{k=0}^{K_v}$ for each $v \in V$ such that $\mathbf{x}_{v,k} = \text{AGG}(\{\mathbf{h}_u \mid u \in \mathcal{N}_k(v)\})$. The maximum hop K_v is dependent on the structure of node v 's neighborhood. These sequences are then processed by a linear RNN, which we name here R for convenience. Finally, the updated representation for each node is obtained through a non-linear transformation of the last hidden state of the RNN.

4.1 PROPERTIES OF RNN-BASED FILTERING OF K -HOP NEIGHBORHOOD

For mini-batch training, we pad shorter sequences with zeros⁵ so that all sequences that are the input to the linear RNN share the same maximum hop K (the sequence length is $K+1$ since the target node itself is included). Then the linear RNN can be seen as a map $R : (\mathbf{x}_{v,0}, \mathbf{x}_{v,1}, \mathbf{x}_{v,2}, \dots, \mathbf{x}_{v,K}) \mapsto \mathbf{s}_{v,K}$, where $v \in V$ is a generic node and $\mathbf{s}_{v,K}$ is the last hidden state of the recurrence $\mathbf{s}_{v,k} = \mathbf{\Lambda} \mathbf{s}_{v,k-1} + \mathbf{W}_{in} \mathbf{x}_{v,K-k}$, with $\mathbf{s}_{v,-1} = \mathbf{0}$. Unrolling the recurrence, we have:

$$\begin{aligned} \mathbf{s}_{v,0} &= \mathbf{W}_{in} \mathbf{x}_{v,K} \\ \mathbf{s}_{v,1} &= \mathbf{\Lambda} \mathbf{W}_{in} \mathbf{x}_{v,K} + \mathbf{W}_{in} \mathbf{x}_{v,K-1} \\ \mathbf{s}_{v,2} &= \mathbf{\Lambda}^2 \mathbf{W}_{in} \mathbf{x}_{v,K} + \mathbf{\Lambda} \mathbf{W}_{in} \mathbf{x}_{v,K-1} + \mathbf{W}_{in} \mathbf{x}_{v,K-2} \\ &\dots \\ \mathbf{s}_{v,K} &= \mathbf{\Lambda}^K \mathbf{W}_{in} \mathbf{x}_{v,K} + \mathbf{\Lambda}^{K-1} \mathbf{W}_{in} \mathbf{x}_{v,K-1} + \dots + \mathbf{\Lambda} \mathbf{W}_{in} \mathbf{x}_{v,1} + \mathbf{W}_{in} \mathbf{x}_{v,0}, \end{aligned} \quad (7)$$

where $\mathbf{x}_{v,k} = \text{AGG}(\{\mathbf{h}_u \mid u \in \mathcal{N}_k(v)\})$. Hence, we have that $\mathbf{s}_{v,K} = \sum_{k=0}^K \mathbf{\Lambda}^k \mathbf{W}_{in} \mathbf{x}_{v,k}$: representations of nodes distant from the target v are scaled by large powers of $\mathbf{\Lambda}$, while the target node itself and the one-hop neighbor representation are scaled by \mathbf{I} and $\mathbf{\Lambda}$, respectively. Under the LRU parametrization (Orvieto et al., 2023b), $\mathbf{\Lambda}$ is initialized and trained to keep entries inside the unit disk (for stability), then $\mathbf{\Lambda}^k$ will induce a decaying structure (*low-pass filter*) over distance. In the limiting case of vanishing $\mathbf{\Lambda}$, the RNN just linearly transforms the representations of each node: $\mathbf{s}_{v,K} = \mathbf{W}_{in} \mathbf{x}_{v,0} = \mathbf{W}_{in} \text{AGG}(\{\mathbf{h}_v\})$.

A surprising property of linear recurrences is that if the hidden state is large enough, *they are injective* — crucial for expressiveness.

Lemma 4.1 (Injectivity of Linear RNNs). *Let $\{\mathbf{x}_v, v \in V : \mathbf{x}_v = (\mathbf{x}_{v,0}, \mathbf{x}_{v,1}, \mathbf{x}_{v,2}, \dots, \mathbf{x}_{v,K_v})\}$ be a set of sequences (with different lengths $K_v \leq K$) of vectors in a (possibly uncountable) set of features $\mathcal{X} \subset \mathbb{R}^d$. Consider a diagonal linear complex-valued RNN with d_s -dimensional hidden state, parameters $\mathbf{\Lambda} \in \text{diag}(\mathbb{C}^{d_s})$, $\mathbf{W}_{in} \in \mathbb{C}^{d_s \times d}$ and recurrence rule $\mathbf{s}_{v,k} = \mathbf{\Lambda} \mathbf{s}_{v,k-1} + \mathbf{W}_{in} \mathbf{x}_{v,K-k}$, initialized at $\mathbf{s}_{v,-1} = \mathbf{0} \in \mathbb{R}^{d_s}$ for all $v \in V$. If $d_s \geq Kd$, then there exist $\mathbf{\Lambda}, \mathbf{W}_{in}$ such that the map $R : (\mathbf{x}_{v,0}, \mathbf{x}_{v,1}, \mathbf{x}_{v,2}, \dots, \mathbf{x}_{v,K}) \mapsto \mathbf{s}_{v,K}$ (with zero right-padding if $K_v < K$) is bijective. Moreover, if the set of RNN inputs has countable cardinality $|\mathcal{X}| = N \leq \infty$, then selecting $d_s \geq d$ is sufficient for the existence of an injective linear RNN mapping R .*

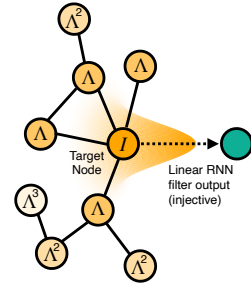


Figure 2: Illustration of filtering induced by a linear RNN, based on distance.

The proof can be found in Appendix A, which leverages the expression $\mathbf{s}_{v,K} = \sum_{k=0}^K \mathbf{\Lambda}^k \mathbf{W}_{in} \mathbf{x}_{v,k}$ and techniques from Orvieto et al. (2023a). Intuitively, this property guarantees that linear RNNs provide representations that retain feature and distance information of K -hop neighbors.

4.2 EXPRESSIVENESS OF GRED

The findings in the last subsection directly imply the following corollary:

⁵If some nodes coincidentally have zero-valued features, we can select a special token which is not in the dictionary of node features as the padding token. In practice, such an operation is not necessary because node representations are first fed into an MLP before the linear RNN, which can learn to shift them away from zero.

Corollary 4.2 (Information kept by GRED). *Assuming wide enough architectural components, then the RNN output at any node $v \in V$, in combination with an injective multiset function AGG aggregating neighbors, is an injective function of the list $(\mathbf{h}_v, \{\mathbf{h}_u \mid u \in \mathcal{N}_1(v)\}, \{\mathbf{h}_u \mid u \in \mathcal{N}_2(v)\}, \dots, \{\mathbf{h}_u \mid u \in \mathcal{N}_{K_v}(v)\})$.*

The corollary, in turn, implies the following result:

Theorem 4.3. *One wide enough GRED layer (linear RNN and injective AGG) is strictly more powerful than one iteration of any 1-hop message passing algorithm.*

Proof. When $K > 1$, the output of one GRED layer at node v , given the injectivity of the linear RNN and AGG, provides a *more fine-grained* characterization of its neighborhood than one-hop message passing which only considers v ’s adjacent neighbors. This means that the output of GRED would change at any perturbation of one-hop neighbors. Moreover, GRED is able to identify two non-isomorphic graphs where 1-WL would fail (see Figure 3 for an example).

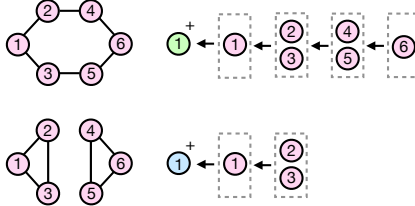


Figure 3: GRED provides distinct updates for the two graphs above. Such graphs, however, are indistinguishable under the 1-WL isomorphism test, assuming (worst-case) nodes have identical features. \square

The expressiveness of GRED is aligned with existing analysis of the general K -hop GNN framework (Feng et al., 2022; Abboud et al., 2022). Notably, GRED aggregates K -hop neighbors in a unique way, i.e., through linear RNNs, which enables GRED to effectively utilize information from distant nodes even when K is large, as supported by the experimental results.

5 EXPERIMENTS

In this section, we evaluate our model on a series of graph benchmarks (Dwivedi et al., 2022a;c). We compare against popular MPNNs including GCN (Kipf & Welling, 2017), GAT (Veličković et al., 2018), GIN (Xu et al., 2019), GatedGCN (Bresson & Laurent, 2017) and PNA (Corso et al., 2020), as well as state-of-the-art graph transformers: Graphormer (Ying et al., 2021), EGT (Hussain et al., 2022), SAT (Chen et al., 2022), GPS (Rampášek et al., 2022) and GRIT (Ma et al., 2023a). We also compare the training time and memory of our model and those of graph transformers to demonstrate the high efficiency of our model. We use three distinct colors to indicate our model, the best graph transformer and the best MPNN. We detail hyper-parameters we use in Appendix C.

Table 1: Test classification accuracy (in percent) of our model and baselines. Performance of baselines is from their original papers (Dwivedi et al., 2022a; Rampášek et al., 2022; Ma et al., 2023a). “-” indicates the baseline didn’t report its performance on that dataset. # params \approx 500K.

Method	Model	MNIST	CIFAR10	PATTERN	CLUSTER
MPNNs	GCN	90.705 \pm 0.218	55.710 \pm 0.381	85.614\pm0.032	69.026 \pm 1.372
	GAT	95.535 \pm 0.205	64.223 \pm 0.455	78.271 \pm 0.186	70.587 \pm 0.447
	GIN	96.485 \pm 0.252	55.255 \pm 1.527	85.590 \pm 0.011	64.716 \pm 1.553
	GatedGCN	97.340\pm0.143	67.312\pm0.311	85.568 \pm 0.088	73.840\pm0.326
GTs	EGT	98.173\pm0.087	68.702 \pm 0.409	86.821 \pm 0.020	79.232 \pm 0.348
	SAN	-	-	86.581 \pm 0.037	76.691 \pm 0.65
	SAT	-	-	86.848 \pm 0.037	77.856 \pm 0.104
	GPS	98.051 \pm 0.126	72.298 \pm 0.356	86.685 \pm 0.059	78.016 \pm 0.180
	GRIT	98.108 \pm 0.111	76.468\pm0.881	87.196\pm0.076	80.026\pm0.277
GRED (Ours)		98.195\pm0.090	75.370\pm0.621	86.759\pm0.020	78.495\pm0.103

Benchmarking GNNs. We first evaluate our model on the node classification datasets: PATTERN and CLUSTER, and graph classification datasets: MNIST and CIFAR10 from Dwivedi et al. (2022a). To get the representation for the entire graph, we simply do average pooling over all node

representations. We train our model four times with different random seeds and report the average accuracy with standard deviation. The comparison with baselines is shown in Table 1. From the table we see that graph transformers generally perform better than MPNNs. Among the four datasets, PATTERN models communities in social networks and all nodes are reachable within 3 hops, which we conjecture is the reason for the marginal performance gap between graph transformers and MPNNs. For a more difficult task, like CIFAR10, that requires information from a relatively larger neighborhood, graph transformers work more effectively. GRED performs well on all four datasets and consistently outperforms MPNNs. Especially, on MNIST GRED achieves the best accuracy, and on CIFAR10 the accuracy of GRED is comparable to GRIT and better than the other graph transformers, which validates that our model can effectively aggregate information beyond the local neighborhood.

Table 2: Test MAE on ZINC 12K. # params \approx 500K.

Model	Test MAE \downarrow
GCN	0.278 \pm 0.003
GAT	0.384 \pm 0.007
GIN	0.387 \pm 0.015
GatedGCN	0.282 \pm 0.015
PNA (Corso et al., 2020)	0.188 \pm 0.004
SAN (Kreuzer et al., 2021)	0.139 \pm 0.006
Graphormer (Ying et al., 2021)	0.122 \pm 0.006
K-subgraph SAT (Chen et al., 2022)	0.094 \pm 0.008
KP-GIN (Feng et al., 2022)	0.093 \pm 0.007
GPS (Rampášek et al., 2022)	0.070 \pm 0.004
PathNN (Michel et al., 2023)	0.090 \pm 0.004
GRIT (Ma et al., 2023a)	0.059 \pm 0.002
GRED (Ours)	0.089 \pm 0.004

Performance on ZINC 12K. Next, we report the test MAE of our model on ZINC 12K (Dwivedi et al., 2022a). The average and standard deviation of four runs with different random seeds are shown in Table 2 along with baseline performance from their original papers. From Table 2 we see that the performance of our model is significantly better than that of MPNNs. Although our performance is worse than the state-of-the-art graph transformer GRIT, our model outperforms some other graph transformer variants (SAN, Graphormer and K-subgraph SAT). This is impressive given that our model doesn’t use any positional encoding, and provides evidence that our model is able to effectively encode graph structural information through the natural inductive bias of recurrence over distance.

Table 3: Test performance on Peptides-func/struct.

Model	Peptides-func Test AP \uparrow	Peptides-struct Test MAE \downarrow
GCN	0.5930 \pm 0.0023	0.3496 \pm 0.0013
GINE	0.5498 \pm 0.0079	0.3547 \pm 0.0045
GatedGCN	0.5864 \pm 0.0077	0.3420 \pm 0.0013
GatedGCN+RWSE	0.6069\pm0.0035	0.3357\pm0.0006
Transformer+LapPE	0.6326 \pm 0.0126	0.2529 \pm 0.0016
SAN+LapPE	0.6384 \pm 0.0121	0.2683 \pm 0.0043
GPS	0.6535 \pm 0.0041	0.2500 \pm 0.0005
GRIT	0.6988\pm0.0082	0.2460\pm0.0012
GRED (Ours)	0.7041\pm0.0049	0.2584\pm0.0015

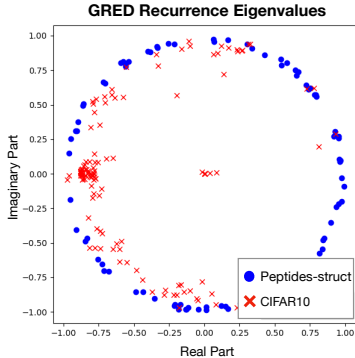


Figure 4: Learned eigenvalues of the first GRED layer: CIFAR10 and Peptides-struct.

Long range graph benchmark. To test the long range modeling capacity of our model, we evaluate it on the Peptides-func and Peptides-struct datasets from Dwivedi et al. (2022c). We follow the

500K parameter budget and train our model four times with different random seeds. The results are shown in Table 3. We observe that GRED significantly outperforms all MPNN baselines. In particular, on Peptides-func GRED even outperforms the best graph transformer GRIT, with no need for positional encoding. GRED’s performance on Peptides-struct is also competitive compared with graph transformers. To illustrate how GRED can learn to encode long-range information, we examine the eigenvalues of the linear recurrent neural network after training, as shown in Figure 4. We observe from the figure that the eigenvalues are pushed close to 1 for the long-range task Peptides-struct, which prevent distant information from decaying too quickly. Compared with Peptides-struct, CIFAR10 requires the model to utilize more information from the local neighborhood, so the magnitudes of the eigenvalues become smaller.

In addition, in Appendix D we show how the performance of our model is affected by the value of K , and the impact of replacing LRU with a vanilla RNN on the performance.

Table 4: Average training time per epoch and GPU memory consumption of GRIT and GRED.

Model	ZINC 12K	CIFAR10	Peptides-func
GRIT	25.6s / 1.9GB	244.4s / 4.6GB	225.6s / 22.5GB
GRED (Ours)	4.1s / 1.4GB	27.8s / 1.4GB	158.9s / 18.5GB
Speedup	6.2 ×	8.8 ×	1.4 ×

Training efficiency. Finally, to demonstrate the high efficiency of our model, we record the average training time per epoch and GPU memory consumption on ZINC, CIFAR10 and Peptides-func. We compare our measurements with those of the state-of-the-art graph transformer GRIT. Both models are trained using a single RTX A5000 GPU with 24GB memory. As shown in Table 4, our model improves the training efficiency by a huge margin, which stems from our compact and parallelizable architecture design.

6 CONCLUSION

In this paper, we introduce the Graph Recurrent Encoding by Distance (GRED) model for graph representation learning. By integrating permutation-invariant neural networks with linear recurrent neural networks, GRED effectively harnesses information from distant nodes without the need for positional encoding or computationally expensive attention mechanisms. Theoretical and empirical evaluations confirm GRED’s superior performance compared with existing MPNNs, and competitive results compared with state-of-the-art graph transformers at a higher training efficiency. This positions GRED as a powerful, efficient, and promising tool for graph representation learning.

REFERENCES

- Ralph Abboud, Radoslav Dimitrov, and Ismail Ilkan Ceylan. Shortest path networks for graph property prediction. In *Learning on Graphs Conference*, 2022.
- Sami Abu-El-Haija, Bryan Perozzi, Amol Kapoor, Nazanin Alipourfard, Kristina Lerman, Hrayr Harutyunyan, Greg Ver Steeg, and Aram Galstyan. Mixhop: Higher-order graph convolutional architectures via sparsified neighborhood mixing. In *ICML*, 2019.
- Uri Alon and Eran Yahav. On the bottleneck of graph neural networks and its practical implications. In *ICLR*, 2021.
- Iz Beltagy, Matthew E Peters, and Arman Cohan. Longformer: The long-document transformer. *arXiv preprint arXiv:2004.05150*, 2020.
- Rajendra Bhatia. *Matrix analysis*. Springer Science & Business Media, 2013.
- Guy E Blelloch. Prefix sums and their applications, 1990.

- Xavier Bresson and Thomas Laurent. Residual gated graph convnets. *arXiv preprint arXiv:1711.07553*, 2017.
- Dexiong Chen, Leslie O’Bray, and Karsten Borgwardt. Structure-aware transformer for graph representation learning. In *ICML, 2022*.
- Rewon Child, Scott Gray, Alec Radford, and Ilya Sutskever. Generating long sequences with sparse transformers. *arXiv preprint arXiv:1904.10509*, 2019.
- Krzysztof Choromanski, Valerii Likhoshesterov, David Dohan, Xingyou Song, Andreea Gane, Tamas Sarlos, Peter Hawkins, Jared Davis, Afroz Mohiuddin, Lukasz Kaiser, et al. Rethinking attention with performers. In *ICLR, 2021*.
- Junyoung Chung, Caglar Gulcehre, Kyunghyun Cho, and Yoshua Bengio. Empirical evaluation of gated recurrent neural networks on sequence modeling. *arXiv preprint arXiv:1412.3555*, 2014.
- Gabriele Corso, Luca Cavalleri, Dominique Beaini, Pietro Liò, and Petar Veličković. Principal neighbourhood aggregation for graph nets. In *NeurIPS, 2020*.
- Tri Dao. Flashattention-2: Faster attention with better parallelism and work partitioning. *arXiv preprint arXiv:2307.08691*, 2023.
- Tri Dao, Dan Fu, Stefano Ermon, Atri Rudra, and Christopher Ré. Flashattention: Fast and memory-efficient exact attention with io-awareness. In *NeurIPS, 2022*.
- Yann N Dauphin, Angela Fan, Michael Auli, and David Grangier. Language modeling with gated convolutional networks. In *ICML, 2017*.
- Jacob Devlin, Ming-Wei Chang, Kenton Lee, and Kristina Toutanova. Bert: Pre-training of deep bidirectional transformers for language understanding. In *NAACL, 2019*.
- Alexey Dosovitskiy, Lucas Beyer, Alexander Kolesnikov, Dirk Weissenborn, Xiaohua Zhai, Thomas Unterthiner, Mostafa Dehghani, Matthias Minderer, Georg Heigold, Sylvain Gelly, et al. An image is worth 16x16 words: Transformers for image recognition at scale. In *ICLR, 2021*.
- Vijay Prakash Dwivedi, Chaitanya K Joshi, Anh Tuan Luu, Thomas Laurent, Yoshua Bengio, and Xavier Bresson. Benchmarking graph neural networks. *JMLR, 2022a*.
- Vijay Prakash Dwivedi, Anh Tuan Luu, Thomas Laurent, Yoshua Bengio, and Xavier Bresson. Graph neural networks with learnable structural and positional representations. In *ICLR, 2022b*.
- Vijay Prakash Dwivedi, Ladislav Rampášek, Michael Galkin, Ali Parviz, Guy Wolf, Anh Tuan Luu, and Dominique Beaini. Long range graph benchmark. In *NeurIPS, 2022c*.
- Jiarui Feng, Yixin Chen, Fuhai Li, Anindya Sarkar, and Muhan Zhang. How powerful are k-hop message passing graph neural networks. In *NeurIPS, 2022*.
- Robert W Floyd. Algorithm 97: shortest path. *Communications of the ACM*, 1962.
- Daniel Y Fu, Tri Dao, Khaled Kamal Saab, Armin W Thomas, Atri Rudra, and Christopher Re. Hungry hungry hippos: Towards language modeling with state space models. In *ICLR, 2023*.
- Justin Gilmer, Samuel S Schoenholz, Patrick F Riley, Oriol Vinyals, and George E Dahl. Neural message passing for quantum chemistry. In *ICML, 2017*.
- Karan Goel, Albert Gu, Chris Donahue, and Christopher Ré. It’s raw! audio generation with state-space models. In *ICML, 2022*.
- Albert Gu, Tri Dao, Stefano Ermon, Atri Rudra, and Christopher Ré. Hippo: Recurrent memory with optimal polynomial projections. In *NeurIPS, 2020*.
- Albert Gu, Karan Goel, and Christopher Re. Efficiently modeling long sequences with structured state spaces. In *ICLR, 2022a*.

- Albert Gu, Ankit Gupta, Karan Goel, and Christopher Ré. On the parameterization and initialization of diagonal state space models. In *NeurIPS*, 2022b.
- Albert Gu, Isys Johnson, Aman Timalsina, Atri Rudra, and Christopher Ré. How to train your hippo: State space models with generalized orthogonal basis projections. In *ICLR*, 2023.
- Ankit Gupta, Albert Gu, and Jonathan Berant. Diagonal state spaces are as effective as structured state spaces. In *NeurIPS*, 2022.
- Ramin Hasani, Mathias Lechner, Tsun-Hsuan Wang, Makram Chahine, Alexander Amini, and Daniela Rus. Liquid structural state-space models. In *ICLR*, 2023.
- Sepp Hochreiter and Jürgen Schmidhuber. Long short-term memory. *Neural computation*, 1997.
- Md Shamim Hussain, Mohammed J Zaki, and Dharmashankar Subramanian. Global self-attention as a replacement for graph convolution. In *SIGKDD*, 2022.
- Jinwoo Kim, Dat Nguyen, Seonwoo Min, Sungjun Cho, Moontae Lee, Honglak Lee, and Seunghoon Hong. Pure transformers are powerful graph learners. In *NeurIPS*, 2022.
- Thomas N Kipf and Max Welling. Semi-supervised classification with graph convolutional networks. In *ICLR*, 2017.
- Nikita Kitaev, Łukasz Kaiser, and Anselm Levskaya. Reformer: The efficient transformer. In *ICLR*, 2020.
- Devin Kreuzer, Dominique Beaini, Will Hamilton, Vincent Létourneau, and Prudencio Tossou. Rethinking graph transformers with spectral attention. *NeurIPS*, 34:21618–21629, 2021.
- Pan Li, Yanbang Wang, Hongwei Wang, and Jure Leskovec. Distance encoding: Design provably more powerful neural networks for graph representation learning. In *NeurIPS*, 2020.
- Zhong Li, Jiequn Han, Weinan E, and Qianxiao Li. Approximation and optimization theory for linear continuous-time recurrent neural networks. *JMLR*, 2022.
- Chris Lu, Yannick Schroecker, Albert Gu, Emilio Parisotto, Jakob Foerster, Satinder Singh, and Fer-
yal Behbahani. Structured state space models for in-context reinforcement learning. In *NeurIPS*, 2023.
- Liheng Ma, Chen Lin, Derek Lim, Adriana Romero-Soriano, Puneet K Dokania, Mark Coates, Philip Torr, and Ser-Nam Lim. Graph inductive biases in transformers without message passing. In *ICML*, 2023a.
- Xuezhe Ma, Chunting Zhou, Xiang Kong, Junxian He, Liangke Gui, Graham Neubig, Jonathan May, and Luke Zettlemoyer. Mega: moving average equipped gated attention. In *ICLR*, 2023b.
- Gaspard Michel, Giannis Nikolentzos, Johannes F Lutzeyer, and Michalis Vazirgiannis. Path neural networks: Expressive and accurate graph neural networks. In *ICML*, 2023.
- Eric Nguyen, Karan Goel, Albert Gu, Gordon W. Downs, Preey Shah, Tri Dao, Stephen A. Baccus, and Christopher Ré. S4nd: Modeling images and videos as multidimensional signals using state spaces. In *NeurIPS*, 2022.
- Giannis Nikolentzos, George Dasoulas, and Michalis Vazirgiannis. k-hop graph neural networks. *Neural Networks*, 2020.
- Antonio Orvieto, Soham De, Caglar Gulcehre, Razvan Pascanu, and Samuel L Smith. On the universality of linear recurrences followed by nonlinear projections. In *ICML Workshop on High-dimensional Learning Dynamics*, 2023a.
- Antonio Orvieto, Samuel L Smith, Albert Gu, Anushan Fernando, Caglar Gulcehre, Razvan Pascanu, and Soham De. Resurrecting recurrent neural networks for long sequences. In *ICML*, 2023b.

- Bo Peng, Eric Alcaide, Quentin Anthony, Alon Albalak, Samuel Arcadinho, Huanqi Cao, Xin Cheng, Michael Chung, Matteo Grella, Kranthi Kiran GV, et al. Rwkv: Reinventing rns for the transformer era. *arXiv preprint arXiv:2305.13048*, 2023.
- Ladislav Rampášek, Michael Galkin, Vijay Prakash Dwivedi, Anh Tuan Luu, Guy Wolf, and Dominique Beaini. Recipe for a general, powerful, scalable graph transformer. In *NeurIPS*, 2022.
- Jimmy TH Smith, Andrew Warrington, and Scott W Linderman. Simplified state space layers for sequence modeling. In *ICLR*, 2023.
- Jie Tang, Jimeng Sun, Chi Wang, and Zi Yang. Social influence analysis in large-scale networks. In *SIGKDD*, 2009.
- Yi Tay, Mostafa Dehghani, Samira Abnar, Yikang Shen, Dara Bahri, Philip Pham, Jinfeng Rao, Liu Yang, Sebastian Ruder, and Donald Metzler. Long range arena: A benchmark for efficient transformers. In *ICLR*, 2021.
- Jake Topping, Francesco Di Giovanni, Benjamin Paul Chamberlain, Xiaowen Dong, and Michael M Bronstein. Understanding over-squashing and bottlenecks on graphs via curvature. In *ICLR*, 2022.
- Hugo Touvron, Louis Martin, Kevin Stone, Peter Albert, Amjad Almahairi, Yasmine Babaei, Nikolay Bashlykov, Soumya Batra, Prajjwal Bhargava, Shruti Bhosale, et al. Llama 2: Open foundation and fine-tuned chat models. *arXiv preprint arXiv:2307.09288*, 2023.
- Ashish Vaswani, Noam Shazeer, Niki Parmar, Jakob Uszkoreit, Llion Jones, Aidan N Gomez, Łukasz Kaiser, and Illia Polosukhin. Attention is all you need. In *NeurIPS*, 2017.
- Petar Veličković, Guillem Cucurull, Arantxa Casanova, Adriana Romero, Pietro Lio, and Yoshua Bengio. Graph attention networks. In *ICLR*, 2018.
- Junxiong Wang, Jing Nathan Yan, Albert Gu, and Alexander M Rush. Pretraining without attention. *arXiv preprint arXiv:2212.10544*, 2022.
- Sinong Wang, Belinda Z Li, Madian Khabsa, Han Fang, and Hao Ma. Linformer: Self-attention with linear complexity. *arXiv preprint arXiv:2006.04768*, 2020.
- Stephen Warshall. A theorem on boolean matrices. *Journal of the ACM (JACM)*, 1962.
- Zhanghao Wu, Zhijian Liu, Ji Lin, Yujun Lin, and Song Han. Lite transformer with long-short range attention. In *ICLR*, 2020.
- Zhanghao Wu, Paras Jain, Matthew Wright, Azalia Mirhoseini, Joseph E Gonzalez, and Ion Stoica. Representing long-range context for graph neural networks with global attention. In *NeurIPS*, 2021.
- Keyulu Xu, Weihua Hu, Jure Leskovec, and Stefanie Jegelka. How powerful are graph neural networks? In *ICLR*, 2019.
- Chengxuan Ying, Tianle Cai, Shengjie Luo, Shuxin Zheng, Guolin Ke, Di He, Yanming Shen, and Tie-Yan Liu. Do transformers really perform badly for graph representation? In *NeurIPS*, 2021.
- Rex Ying, Ruining He, Kaifeng Chen, Pong Eksombatchai, William L Hamilton, and Jure Leskovec. Graph convolutional neural networks for web-scale recommender systems. In *SIGKDD*, 2018.
- Manzil Zaheer, Satwik Kottur, Siamak Ravanbakhsh, Barnabas Poczos, Russ R Salakhutdinov, and Alexander J Smola. Deep sets. In *NeurIPS*, 2017.
- Bohang Zhang, Shengjie Luo, Liwei Wang, and Di He. Rethinking the expressive power of gnns via graph biconnectivity. In *ICLR*, 2023.
- Nicolas Zucchet, Seijin Kobayashi, Yassir Akram, Johannes von Oswald, Maxime Larcher, Angelika Steger, and João Sacramento. Gated recurrent neural networks discover attention. *arXiv preprint arXiv:2309.01775*, 2023a.
- Nicolas Zucchet, Robert Meier, Simon Schug, Asier Mujika, and João Sacramento. Online learning of long range dependencies. *arXiv preprint arXiv:2305.15947*, 2023b.

A PROOFS

Lemma 4.1 (Injectivity of Linear RNNs). *Let $\{\mathbf{x}_v, v \in V : \mathbf{x}_v = (\mathbf{x}_{v,0}, \mathbf{x}_{v,1}, \mathbf{x}_{v,2}, \dots, \mathbf{x}_{v,K_v})\}$ be a set of sequences (with different lengths $K_v \leq K$) of vectors in a (possibly uncountable) set of features $\mathcal{X} \subset \mathbb{R}^d$. Consider a diagonal linear complex-valued RNN with d_s -dimensional hidden state, parameters $\mathbf{\Lambda} \in \text{diag}(\mathbb{C}^{d_s})$, $\mathbf{W}_{in} \in \mathbb{C}^{d_s \times d}$ and recurrence rule $\mathbf{s}_{v,k} = \mathbf{\Lambda} \mathbf{s}_{v,k-1} + \mathbf{W}_{in} \mathbf{x}_{v,K_v-k}$, initialized at $\mathbf{s}_{v,-1} = \mathbf{0} \in \mathbb{R}^{d_s}$ for all $v \in V$. If $d_s \geq Kd$, then there exist $\mathbf{\Lambda}, \mathbf{W}_{in}$ such that the map $R : (\mathbf{x}_{v,0}, \mathbf{x}_{v,1}, \mathbf{x}_{v,2}, \dots, \mathbf{x}_{v,K}) \mapsto \mathbf{s}_{v,K}$ (with zero right-padding if $K_v < K$) is bijective. Moreover, if the set of RNN inputs has countable cardinality $|\mathcal{X}| = N \leq \infty$, then selecting $d_s \geq d$ is sufficient for the existence of an injective linear RNN mapping R .*

Proof. For now, let us assume for ease of exposition that all sequences are of length K . Also, let us, for simplicity, drop the dependency on $v \in V$ and talk about generic sequences.

The proof simply relies on the idea of writing the linear recurrence in matrix form (Orvieto et al., 2023a; Gu et al., 2022b). Note that for a generic input $\mathbf{x} = (\mathbf{x}_0, \mathbf{x}_1, \mathbf{x}_2, \dots, \mathbf{x}_K) \in \mathbb{R}^{d \times (K+1)}$, the recurrence output can be rewritten in terms of powers of $\mathbf{\Lambda} = \text{diag}(\lambda_1, \lambda_2, \dots, \lambda_{d_s})$ as follows (see Sec. 4):

$$\mathbf{s}_K = \sum_{k=0}^K \mathbf{\Lambda}^k \mathbf{W}_{in} \mathbf{x}_k. \quad (8)$$

We now present sufficient conditions for the map $R : (\mathbf{x}_0, \mathbf{x}_1, \mathbf{x}_2, \dots, \mathbf{x}_K) \mapsto \mathbf{s}_K$ to be injective or bijective. The proof for bijectivity does not require the set of node features to be in a countable set, and it is simpler.

Bijective mapping. First, let us design a proper matrix $\mathbf{W}_{in} \in \mathbb{R}^{d_s \times d}$. We choose $d_s = (K+1)d$ and set $\mathbf{W}_{in} = \mathbf{I}_{d \times d} \otimes \mathbf{1}_{(K+1) \times 1}$. As a result, the RNN will independently process each sequence dimension with a sub-RNN of size K . The resulting $\mathbf{s}_K \in \mathbb{R}^{(K+1)d}$ will gather each sub-RNN output by concatenation. We can then restrict our attention to the first components of the input sequence.

$$(\mathbf{s}_K)_{1:(K+1)} = \sum_{k=0}^K \text{diag}(\lambda_1, \lambda_2, \dots, \lambda_{d_s})^k \mathbf{1}_{(K+1) \times 1} x_{k,1}. \quad (9)$$

This sum can be written conveniently with multiplications using a Vandermonde matrix:

$$(\mathbf{s}_L)_{1:(K+1)} = \begin{pmatrix} \lambda_1^K & \lambda_1^{K-1} & \dots & \lambda_1 & 1 \\ \lambda_2^K & \lambda_2^{K-1} & \dots & \lambda_2 & 1 \\ \vdots & \vdots & \ddots & \vdots & \vdots \\ \lambda_{K+1}^K & \lambda_{K+1}^{K-1} & \dots & \lambda_{K+1} & 1 \end{pmatrix} \mathbf{x}_{0:K,1}^{\leftarrow}. \quad (10)$$

where $\mathbf{x}_{0:K,1}^{\leftarrow}$ is the input with reversed arrow of time. The proof is concluded by noting that Vandermonde matrices of size $(K+1) \times (K+1)$ are full-rank since they have non-zero determinant $\prod_{1 \leq i < j \leq d_s} (\lambda_i - \lambda_j) \neq 0$, under the assumption that all λ_i are distinct. Note that one does not need complex eigenvalues to achieve this, both $\mathbf{\Lambda}$ and \mathbf{W}_{in} are real. However, as discussed in (Orvieto et al., 2023a), complex eigenvalues improve conditioning of the Vandermonde matrix.

Injective mapping. The condition for injectivity is that if $\mathbf{x} \neq \hat{\mathbf{x}}$, then $R(\mathbf{x}) \neq R(\hat{\mathbf{x}})$. In formulas,

$$\mathbf{s}_K - \hat{\mathbf{s}}_K = \sum_{k=0}^K \mathbf{\Lambda}^k \mathbf{W}_{in} (\mathbf{x}_k - \hat{\mathbf{x}}_k) \neq 0 \quad (11)$$

Let us assume the state dimension coincides with the input dimension, and let us set $\mathbf{W}_{in} = \mathbf{I}_{d \times d}$. Then, we have the condition

$$\mathbf{s}_K - \hat{\mathbf{s}}_K = \sum_{k=0}^K \mathbf{\Lambda}^k (\mathbf{x}_k - \hat{\mathbf{x}}_k) \neq 0. \quad (12)$$

Since $\mathbf{\Lambda} = \text{diag}(\lambda_1, \lambda_2, \dots, \lambda_{d_s})$ is diagonal, we can study each component of $\mathbf{s}_K - \hat{\mathbf{s}}_K$ separately. We therefore require

$$s_{K,i} - \hat{s}_{K,i} = \sum_{k=0}^K \lambda_i^k (x_{k,i} - \hat{x}_{k,i}) \neq 0 \quad \forall i \in \{1, 2, \dots, d\}. \quad (13)$$

We can then restrict our attention to linear one-dimensional RNNs (i.e. filters) with one-dimensional input $\mathbf{x} \in \mathbb{R}^{1 \times (K+1)}$. We would like to choose $\lambda \in \mathbb{C}$ such that

$$\sum_{k=0}^K \lambda^k (x_k - \hat{x}_k) \neq 0 \quad (14)$$

Under the assumption $|\mathcal{X}| = N \leq \infty$, $\mathbf{x} - \bar{\mathbf{x}}$ is a generic signal in a countable set ($N(N-1)/2 = \Omega(N^2)$ possible choices). Let us rename $\mathbf{z} := \mathbf{x} - \bar{\mathbf{x}} \in \mathcal{Z} \subset \mathbb{R}^{1 \times (K+1)}$, $|\mathcal{Z}| = \Omega(N^2)$. We need

$$\langle \bar{\boldsymbol{\lambda}}, \mathbf{z} \rangle \neq 0, \quad \forall \mathbf{z} \in \mathcal{Z}, \quad \text{where } \bar{\boldsymbol{\lambda}} = (1, \lambda, \lambda^2, \dots, \lambda^K) \quad (15)$$

Such λ can always be found *in the real numbers*, and the reason is purely geometric. We need

$$\bar{\boldsymbol{\lambda}} \notin \mathcal{Z}_\perp := \bigcup_{\mathbf{z} \in \mathcal{Z}} \mathbf{z}_\perp.$$

Note that $\dim(\mathbf{z}_\perp) = K$, so $\dim(\mathcal{Z}_\perp) = K$ due to the countability assumption — in other words the Lebesgue measure vanishes: $\mu(\mathcal{Z}_\perp; \mathbb{R}^{K+1}) = 0$. If $\bar{\boldsymbol{\lambda}}$ were an arbitrary vector, we would be done since we can pick it at random and with probability one $\bar{\boldsymbol{\lambda}} \notin \mathcal{Z}_\perp$. But $\bar{\boldsymbol{\lambda}}$ is structured (lives on a 1-dimensional manifold), so we need one additional step.

Note that $\bar{\boldsymbol{\lambda}}$ is parametrized by λ , and in particular $\mathbb{R} \ni \lambda \mapsto \bar{\boldsymbol{\lambda}} \in \mathbb{R}^{K+1}$ is a curve in \mathbb{R}^{K+1} , we denote this as γ_λ . Now, crucially, note that the support of γ_λ is a smooth curved manifold for $K > 1$. In addition, crucially, $0 \notin \gamma_\lambda$. We are done: it is impossible for the γ_λ curve to live in a K dimensional space composed of a union of hyperplanes; it indeed has to span to whole \mathbb{R}^{K+1} , without touching the zero vector (see Figure 5). The reason why it spans the whole \mathbb{R}^{K+1} comes from the Vandermonde determinant! Let $\{\lambda_1, \lambda_2, \dots, \lambda_K\}$ be a set of K distinct λ values. The Vandermonde matrix

$$\begin{pmatrix} \lambda_1^K & \lambda_1^{K-1} & \dots & \lambda_1 & 1 \\ \lambda_2^K & \lambda_2^{K-1} & \dots & \lambda_2 & 1 \\ \vdots & \vdots & \ddots & \vdots & \vdots \\ \lambda_K^{K+1} & \lambda_K^{K-2} & \dots & \lambda_K & 1 \end{pmatrix}$$

has determinant $\prod_{1 \leq i < j \leq d_s} (\lambda_i - \lambda_j) \neq 0$ — its full rank, meaning that the vectors $\bar{\boldsymbol{\lambda}}_1, \bar{\boldsymbol{\lambda}}_2, \dots, \bar{\boldsymbol{\lambda}}_{K+1}$ span the whole \mathbb{R}^{K+1} . note that $\lambda \mapsto \bar{\boldsymbol{\lambda}}$ is a continuous function, so even though the single $\bar{\boldsymbol{\lambda}}_i$ might live on \mathcal{Z}_\perp there exist a value in between them which is not contained in \mathcal{Z}_\perp .

□

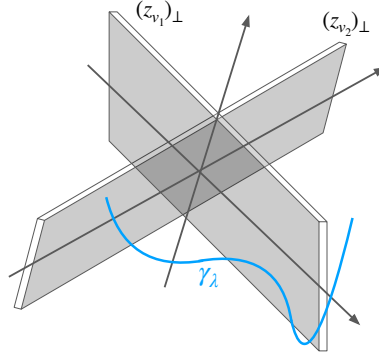


Figure 5: Proof illustration for Proposition 4.1 (injectivity proof). The set \mathcal{Z}_{\perp} is depicted as union of hyperplanes, living in \mathbb{R}^{K+1} and here sketched in three dimensions. The curve $\gamma_{\gamma} : \gamma \mapsto (1, \gamma, \gamma^2, \dots, \gamma^K)$ is shown as a blue line. The proof shows that, for $\gamma \in \mathbb{R}$, the support of γ_{λ} is not entirely contained in \mathcal{Z}_{\perp} .

B SIMPLIFIED IMPLEMENTATION OF ONE GRED LAYER

```

1 import jax.numpy as jnp
2 import flax.linen as nn
3 from typing import Callable
4
5 class MLP(nn.Module):
6     dim_h: int
7     drop_rate: float = 0.
8
9     @nn.compact
10    def __call__(self, inputs, training: bool = False):
11        x = nn.LayerNorm()(inputs)
12        x = nn.Dense(self.dim_h)(x)
13        x = nn.gelu(x)
14        x = nn.Dropout(self.drop_rate, deterministic=not training)(x)
15        x = nn.Dense(self.dim_h)(x)
16        x = nn.Dropout(self.drop_rate, deterministic=not training)(x)
17        return x + inputs
18
19 def binary_operator_diag(element_i, element_j):
20     # Binary operator for parallel scan of linear recurrence.
21     a_i, bu_i = element_i
22     a_j, bu_j = element_j
23     return a_j * a_i, bu_i * a_j + bu_j
24
25 class LRU(nn.Module):
26     dim_v: int # State dimension
27     dim_h: int
28     drop_rate: float
29     init_eigenvalue_magnitude: Callable
30     init_eigenvalue_phase: Callable
31     init_kernel: Callable
32
33     @nn.compact
34     def __call__(self, inputs, training: bool = False):
35         # Shape of inputs: (K+1, batch_size, num_nodes, dim_h)
36         xs = nn.LayerNorm()(inputs)
37
38         # Construct Lambda:
39         nu_log = self.param("nu_log", self.init_eigenvalue_magnitude, (self.dim_v,))
40         theta_log = self.param("theta_log", self.init_eigenvalue_phase, (self.dim_v,))
41         diag_lambda = jnp.exp(-jnp.exp(nu_log) + 1j * jnp.exp(theta_log))
42
43         # Construct W_in:
44         W_in_re = self.param("W_in_re", self.init_kernel, (self.dim_h, self.dim_v))
45         W_in_im = self.param("W_in_im", self.init_kernel, (self.dim_h, self.dim_v))
46         W_in = W_in_re + 1j * W_in_im
47
48         # Parallel scan over the sequence of length K+1:
49         xs = xs @ W_in
50         lambdas = jnp.repeat(diag_lambda[None, ...], inputs.shape[0], axis=0)
51         lambdas = jnp.expand_dims(lambdas, axis=(1, 2))

```

```

52     _, xs = jax.lax.associative_scan(binary_operator_diag, (lambdas, xs), reverse=True)
53     x = xs[0]
54
55     # Project the complex-valued hidden state to real:
56     W_out_re = self.param("W_out_re", self.init_kernel, (self.dim_v, self.dim_h))
57     W_out_im = self.param("W_out_im", self.init_kernel, (self.dim_v, self.dim_h))
58     W_out = W_out_re + 1j * W_out_im
59     x = nn.gelu((x @ W_out).real)
60
61     # Apply GLU:
62     x = nn.Dropout(self.drop_rate, deterministic=not training)(x)
63     x = nn.Dense(self.dim_h)(x) * jax.nn.sigmoid(nn.Dense(self.dim_h)(x))
64     x = nn.Dropout(self.drop_rate, deterministic=not training)(x)
65     return x + inputs[0]
66
67 class GRED(nn.Module):
68     dim_v: int # State dimension
69     dim_h: int
70     drop_rate: float
71     init_eigenvalue_magnitude: Callable
72     init_eigenvalue_phase: Callable
73     init_kernel: Callable
74
75     @nn.compact
76     def __call__(self, inputs, dist_masks, training: bool = False):
77         # Shape of inputs: (batch_size, num_nodes, dim_h)
78         # Shape of dist_masks: (batch_size, K+1, num_nodes, num_nodes)
79         xs = jnp.swapaxes(dist_masks, 0, 1) @ inputs
80         xs = MLP(self.dim_h, self.drop_rate)(xs)
81         x = LRU(
82             self.dim_v,
83             self.dim_h,
84             self.drop_rate,
85             self.init_eigenvalue_magnitude,
86             self.init_eigenvalue_phase,
87             self.init_kernel
88         )(xs, training=training)
89         return x

```

C HYPERPARAMETERS

Table 5: Hyperparameters for GRED. “-” indicates that K is the diameter of the graph.

Hyperparameter	ZINC 12K	MNIST	CIFAR10	PATTERN	CLUSTER	Peptides
# Layers	11	4	8	10	16	8
K	4	2	4	-	-	40
Dropout	0.2	0.15	0.15	0.2	0.2	0.2
d	72	128	96	64	64	88
d_s	72	128	64	64	64	88
Learning rate	0.001	0.001	0.001	0.001	0.001	0.001
Weight decay	0.1	0.1	0.1	0.1	0.1	0.2
# Epochs	2000	200	200	100	100	200
Batch size	32	16	16	32	32	32

D ADDITIONAL EXPERIMENTS

Effect of K on performance. We show how different K values affect the performance of GRED on CIFAR10 (Table 6), ZINC (Table 7) and Peptides-func (Table 8). We use K_{\max} to denote the maximum diameter of all graphs in the dataset. For Peptides-func, the maximum K we tried was smaller than K_{\max} in order to fit the model into a single RTX A5000 GPU with 24GB memory. From the three tables, we can observe that larger K values generally yield better performance. On CIFAR10 and ZINC, while directly using K_{\max} already outperforms MPNNs, the optimal value of K yielding best performance lies strictly between 1 and K_{\max} . This may be because information that is too far away is less important for these two tasks (interestingly, the best K value for CIFAR10 is similar to the width of a convolutional kernel on a normal image). On Peptides-func, the change of performance is more monotonic in K . When $K = 40$, GRED outperforms the best graph transformer GRIT. This result is impressive considering that GRED doesn't use any positional encoding, and further validates that the architecture of GRED alone can encode the graph structure. We observe no further performance gain when we increase K to 60.

Table 6: Effect of K on the performance on CIFAR10.

K	1	4	7	$K_{\max}=10$
Test Acc (%)	72.540±0.336	75.370±0.621	74.490±0.335	74.210±0.274

Table 7: Effect of K on the performance on ZINC.

K	1	2	4	8	$K_{\max}=22$
Test MAE ↓	0.231±0.002	0.161±0.003	0.089±0.004	0.108±0.004	0.131±0.008

Table 8: Effect of K on the performance on Peptides-func.

K	5	10	20	40	60
Test AP ↑	0.6657±0.0069	0.6883±0.0076	0.6960±0.0060	0.7041±0.0049	0.7031±0.0017

Vanilla RNN vs LRU. We replace the LRU component (5) of GRED with a vanilla RNN:

$$\mathbf{s}_{v,k}^{(\ell)} = \tanh \left(\mathbf{W}_{\text{rec}} \mathbf{s}_{v,k-1}^{(\ell)} + \mathbf{W}_{\text{in}} \mathbf{x}_{v,K-k}^{(\ell)} \right), \quad (16)$$

where $\mathbf{W}_{\text{rec}} \in \mathbb{R}^{d_s \times d_s}$ and $\mathbf{W}_{\text{in}} \in \mathbb{R}^{d_s \times d}$ are two trainable real weight matrices, and show the difference in performance in Table 9. We use the same number of layers and the same K for both models. We can observe that the performance of GRED with a vanilla RNN drops significantly. On CIFAR10 and ZINC where K is small, GRED_{RNN} still outperforms the best MPNN. However, on Peptides-func where we use 8 layers and $K = 40$ per layer, the vanilla RNN becomes difficult to train and the performance of GRED_{RNN} is even worse than the best MPNN.

Table 9: Performance of GRED using vanilla RNN or LRU.

	CIFAR10 ↑	ZINC ↓	Peptides-func ↑
Best MPNN	67.312±0.311	0.188±0.004	0.6069±0.0035
GRED_{RNN}	69.215±0.080	0.160±0.005	0.4945±0.0024
GRED_{LRU}	75.370±0.621	0.089±0.004	0.7041±0.0049

Performance on TUDataset. We further evaluate GRED on NCI1 and PROTEINS from TUDataset. We follow the experimental setup of Abboud et al. (2022), and report the average accuracy and standard deviation of 10 splits, as shown in Table 10. Baseline performance is reported by Abboud et al. (2022). Our model generalizes well to TUDataset and shows good performance. Furthermore, GRED outperforms SPN (Abboud et al., 2022) with the same number of hops, which validates that GRED is a more effective architecture for utilizing information from a large neighborhood.

Table 10: Performance (accuracy) of GRED on TUDataset.

Model	NCI1	PROTEINS
DGCNN	76.4±1.7	72.9±3.5
DiffPool	76.9±1.9	73.7±3.5
ECC	76.2±1.4	72.3±3.4
GIN	80.0±1.4	73.3±4.0
GraphSAGE	76.0±1.8	73.0±4.5
SPN (Abboud et al., 2022) ($K = 10$)	78.2±1.2	74.5±3.2
GRED ($K = 10$)	82.6±1.4	75.0±2.9